DOR: 20.1001.1.27170314.2022.11.4.2.4

Research Paper

Enhanced Microstructure and Mechanical Properties of A216 Steel by Friction Stir Processing

Gholamreza Khalaj[1*], Gholamreza Ghaffari[2], Bahram Abdolmaleki[2]
[1]Department of Engineering, Saveh Branch, Islamic Azad University, Saveh, Iran
[2]Arak Godazesh Company, Arak, Iran
[*]Email of Corresponding Author: gh.khalaj@srbiau.ac.ir
Received: November 13, 2022; Accepted: December 21, 2022

Abstract
One of the main problems in oil and gas pipelines is abrasion corrosion on the edges of the flow channel in the plug and ball valves. Under normal conditions, the gas is moving at a pressure of about 145 bar and an approximate speed of 70 feet per second; the suspended particles in the gas collide with the edges of the flow channel and cause severe erosion on them. The abrasion resistance of steels depends mainly on their surface properties and can be increased by increasing the surface hardness by friction stir processing (FSP). In this study, A216-WCB steel, which is used in the manufacturing of casting parts for valves, flanges, and fittings, was processed using an FSP for one and three passes. The microstructure, hardness, and wear properties of the processed area were investigated. The results showed that two distinct zones, the stir zone (SZ) and the thermo-mechanical affected zone (TMAZ), are formed in the processed zone. Due to the FSP, the grain size in the stirring region decreased from 25 microns to about 3 microns. The hardness of the SZ increased from 165 Vickers to about 784 HV. Tensile strength increased by 24%, and elongation was reduced by 25% for the processed sample compared to the raw metal. This may be due to phase transformation to martensite and grain size refinement. Also, the abrasion resistance of the stirring area increased up to 2.5 times.

Keywords
Friction Stir Process, Wear Resistance, Low-carbon Steel, Phase Transformation, Mechanical Properties

1. Introduction

Corrosion causes a lot of annual damage in various industries, mainly in the oil, gas, and petrochemical industries. One example of corrosion is abrasion corrosion with fluid flow. Fluids can be liquid or gaseous. Crude natural gas extracted from wells carries with it quantities of sand, gravel, and salt water, which are refined in gas refineries before being sent to consumption points. The presence of these solid particles along with water that can turn into hydrated ice at low temperatures has adverse effects on lines and facilities, especially gas valves, which require a lot of time and money to compensate. Unfortunately, some of these impurities remain in the fluid even after refining and are sent to the consumption points and pressure-reducing stations of the pipelines along with the gas and due to consecutive intersections in these stations, it causes abrasion corrosion [1].

Gas valves are equipment in today's industry that is responsible for shutting off and connecting the flow or regulating the flow and pressure of the fluid. The main and important functions of valves used, especially in the oil and gas industry, are: switching off and on the flow of liquids and gases, regulating the passage of the required amount of liquids and gases, regulating and controlling the amount and pressure of liquids and gases to the required level. The most important part of the valves that are in direct contact with the fluid is the wedge. There are various methods to prevent corrosion of the wedges, including the creation of a layer (Cladding) with the process of gas tungsten arc welding (GTAW) and gas metal arc welding (GMAW) or the creation of metal matrix composites with ceramic reinforcements [2]. Although these methods have many advantages, they also have many disadvantages; including fabrication cost, spraying of welding materials, and distortion due to welding operations. To solve these problems, a new method based on sever plastic deformation in a solid state was proposed [3].

Although most of the efforts made in the field of friction stir welding /processing (FSW/P) have been focused on aluminum alloys, steels have also attracted the attention of many researchers. Due to the lower heat input resulting from FSW/P (compared to fusion welding processes), metallurgical changes in the HAZ are expected to be reduced, and distortions and residual stresses in steels will be minimized. This issue is very important in welding thick sections (shipbuilding and heavy industries). Apart from this, due to the solid-state nature of the FSW/P, the problems related to hydrogen embrittlement in steels are solved. In addition, in the solid state process of FSW/P, there is no problem with welding fumes, especially fumes containing hexavalent Cr. These advantages have made the use of FSW/P attractive for joining/surface-treating steel parts in many applications [4]. The FSPed workpiece generally has good hardness, transverse tensile properties, bending properties, and impact toughness. By conducting transverse tensile tests, it was shown that the yield and final strength of the SZ are usually higher than the BM, and the failure occurs in the BM, while the flexibility of both is almost equal [5,6]. It was also shown that the hardness of the SZ is much higher than the BM, which is compatible with the tensile strength results [7]. The friction stir process is used to modify the surfaces of different steels and create some mechanical or corrosion properties.

The basic concept of FSP is that a rotating tool consisting of a pin and a shoulder penetrates the surface of the material and travels in a specific direction to cover the desired area. During the FSP process, the workpiece undergoes severe plastic deformation at high temperatures, in which dynamic grain recrystallization occurs. Severe plastic deformation and exposure to thermal stress lead to significant changes in the surface microstructure of the material. As a result, two main zones are formed: the SZ and the TMAZ. With the combined effects of severe plastic deformation and dynamic recrystallization, a microstructure with refined and coaxial grains in the size range of 1.0 to 10 μm is created. FSP has been used in many studies and therefore more detailed information on the principles of processing and its benefits can be found in previous literature. Although there are many articles about the FSP of non-ferrous metals, especially aluminum, relatively few articles have been published about the FSP of steel[8-12].

FSP has been applied to increase the surface abrasion resistance of duplex UNS S32205 steel and ASTM 743 steel [13,14]. The processed surfaces were tested under severe pitting erosion conditions and a significant improvement in abrasion resistance was reported for both processed materials. FSP has also been successfully used in the processing of 1080 carbon steel, SKD61 tool steel, IF steel,

super-austenitic steel, AISI 420 martensitic steel, and AISI D2 tool steel [15-19]. Aldajah et al. [15] investigated the role of FSP on the wear properties of 1080 steel. In this research, 1080 carbon steel was subjected to a friction stir process. Investigations showed that the pearlite structure changed to martensite and as a result, the hardness of the sample increased significantly. This increase improved the wear and friction behavior of steel. Then the wear behavior was investigated in two types dry wear and wear with lubrication. It was seen that in the dry state, FSP reduced the friction coefficient by 25% and the wear rate by about 10 times, but in the lubricated state, it had a small effect on the friction coefficient and reduced the wear rate by four times. In another research, Chen et al. FSPed SKD61 tool steel and investigated the microstructure, tensile properties, and wear properties. As a result of FSP, fine grains with the martensitic structure were formed, which increased the hardness. The lower the heat input, the finer the grains. The width and depth of the abrasion test in the FSP sample were reduced by 62% and 86%, respectively, compared to the original steel. Also, all the tensile samples broke from the BM. Therefore, they concluded that the production of a fine-grained martensitic structure is an effective method for creating a structure with good tensile and wear-resistant properties [16].

Singh et al. investigated the friction stir process on SA210 Grade A1 low-carbon steel used in boilers. The rotation speeds of tungsten carbide tools were 800 and 1400 rpm and the processes were performed with a forward speed of 40 mm/min in two passes. Based on the increase in tool rotation speed, the grain size decreased from 25 microns in the BM to 7.8 and 5.9 microns in the SZ, respectively. Also, the microhardness of 180 Vickers in the BM increased 1.72 and 2.38 times, respectively. They stated that the reasons for the increase in hardness and tensile strength are the grain refining and phase change from austenite at the process temperature to martensite and ferrite. In another study, they were able to achieve a structure with a grain size of about 1 micron and a hardness of 2.5 times by increasing the tool rotation speed to 1900 rpm and three passes with a forward speed of 20 mm/min [21, 20].

Sekban et al. [22] performed a friction stir process on low-carbon steel ABS-P2-96 Gr A that was able to reduce the grain size from 25 microns to 5 microns. The rotation speed of the tungsten carbide tool was 635 rpm and the forward speed was 45 mm/min. Tensile strength increased by 20% and hardness increased from 140 Vickers in the BM to 200 Vickers in the SZ. Also, the average coefficient of friction is reduced from 0.46 to 0.42 and the amount of weight loss in the wear test is reduced by half. The effect of FSP on the pitting erosion properties of 13Cr4Ni steel used in water turbines was also studied in another research [14]. Microstructure studies showed that due to FSP, the microstructure is modified and the grain size is reduced by 10 times. Also, the size of some grains reached below micrometer. The hardness increased by 2.6 times and the pitting erosion resistance increased by 2.4 times.

The main purpose of the present study is to apply the FSP process on plain carbon steel to modify the microstructure and evaluate changes in wear behavior. In this study, cast steel sheet A216-WCB was subjected to a friction stir process (FSP) in water. Tungsten carbide (WC) tool was used. Structural characterizations were performed by scanning electron microscopy (SEM) and light microscopy (OM). The results show that, due to this process, the grain size is reduced and the ferrite-pearlite phase is changed to martensite. The results of hardness, tensile, and wear resistance tests show that

the hardness of the processed area has increased 4.75 times compared to the BM and the wear resistance has increased 2.5 times.

2. Materials and methods

In the present study, to investigate the effect of the friction stir process (FSP) on the microstructure, microhardness, and wear behavior of the BM, A216-WCB cast steel (hereafter denoted as A 216) in the shape of 150 × 150 × 6 mm was used (Figure 1a). Chemical composition of A216 is 0.26C, 0.96Mn, 0.49Si and Fe (%wt).

The tungsten carbide tool (WC grade H) with a tool shoulder 20 mm in diameter and a conical pin with a large diameter of 7 mm and a small diameter of 5 mm was used for FSP, as shown in Figure (1b). The FSP tests were performed with a rotation speed of 2800 rpm, a transverse speed of 80 mm/min, a tool plunge depth of 2 mm, and a 3° tilt angle in water at 5 °C. The FSP was performed on the surfaces with 1 to 3 passes at a similar process condition (called P1 and P3).

To examine the microstructure, the cross-section of FSPed samples was cut by a wire cut machine (Figure 1c) and mechanically ground with 120 to 1500-grade SiC papers and polished with 1.6 and 0.25 µm diamond paste. Subsequently, they were etched in 2% nital solution for about 5 s. Optical microscopy (OLYMPUS model BX60) and field emission scanning electron microscopy (FESEM model TESCAN MIRA3) were used to study microstructural characterization. The average grain size was determined based on the ASTM E112 standard.

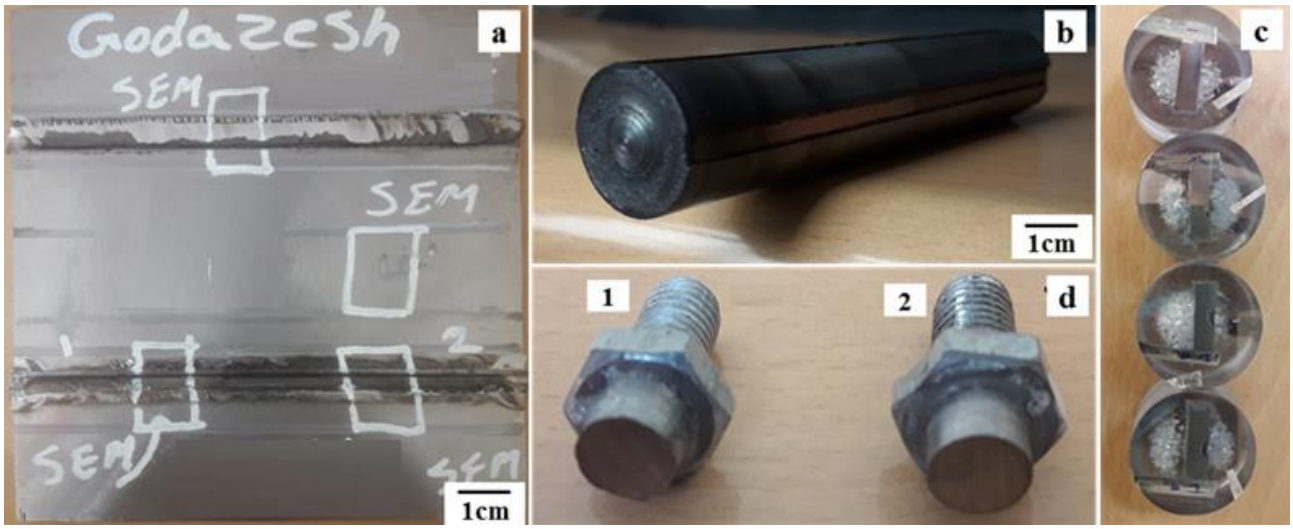

Figure 1. (a) Sample piece after FSP process, (b) Friction stir process tool used, (c) Metallographic samples from the created layers, (d) wear test specimens, No. 1 BM and No. 2, P1 specimen

Vicker microhardness (Anton Paar model MHT-10), tensile (Santam model STM-600) and wear test, was used for mechanical properties characterization of the FSPed samples. The Vickers microhardness (HV) profiles in SZ, TMAZ, and BM were carried out on the cross-section of the samples which was perpendicular to the traverse direction of the FSP with a load of 300g and a dwelling time of 10 s. The microhardness was measured at the distance of 100 µm below the processed surface at about 200 µm between each measurement based on the E384 standard. The tensile tests were conducted on a universal testing machine based on the ASTM E8 standard. The BM and FSPed specimens of 6 × 25 × 3.8 mm were made. Tensile tests were performed at a strain rate of

1×10^{-3} s^{-1}. A wear test was performed with a pin-on-disk device under the constant force of 80 kg, linear disc velocity of 1280 m/min, and applied stress of 14,500 kPa based on the ASTM G99 standard. The weight loss of each sample was measured after distances of 600, 1200, 1800, 2400, and 3000 meters.

3. Results and Discussion

3.1 Microstructure

Light microscope images showing the microstructure of base steel and FSPed samples are shown in Figure 2. The microstructure created in FSP is usually divided and studied into two parts: the stir zone (SZ) and the thermo-mechanical affected zone (TMAZ). Figure 2(a) shows the general view of different areas of the P1 sample. Different parts of the SZ, TMAZ, and base metal (BM) are named on the image. Hardness measurement locations are marked with red circles. Figure 2(b) shows the structure of the SZ, identified in Figure 2(a) at higher magnification. The structure in this region consists of martensite. Figure 2(c) shows the boundary structure of TMAZ area and base steel with non-coaxial ferrite and pearlite structure. Figure 2(d) shows the general view of the different regions of the P3 sample. Figure 2(e) shows the structure of the SZ of the P3 sample in higher magnification, which includes martensite. Figure 2(f) shows the BM structure. The microstructure of base steel consists of coaxial ferrite and pearlite and with equivalent carbon of 0.44%, the almost equilibrium structure of base steel includes 55% pearlite and 45% ferrite. The friction stir processing leads to a significant modification in the microstructure, especially inside the SZ. After treatment, the average grain size decreased from 25 μm in the BM to about 3 μm in the stirred zone. Coarse grains of ferrite and pearlite were crushed and fined under the influence of severe plastic deformation and dynamic recrystallization during the processing [22, 21].

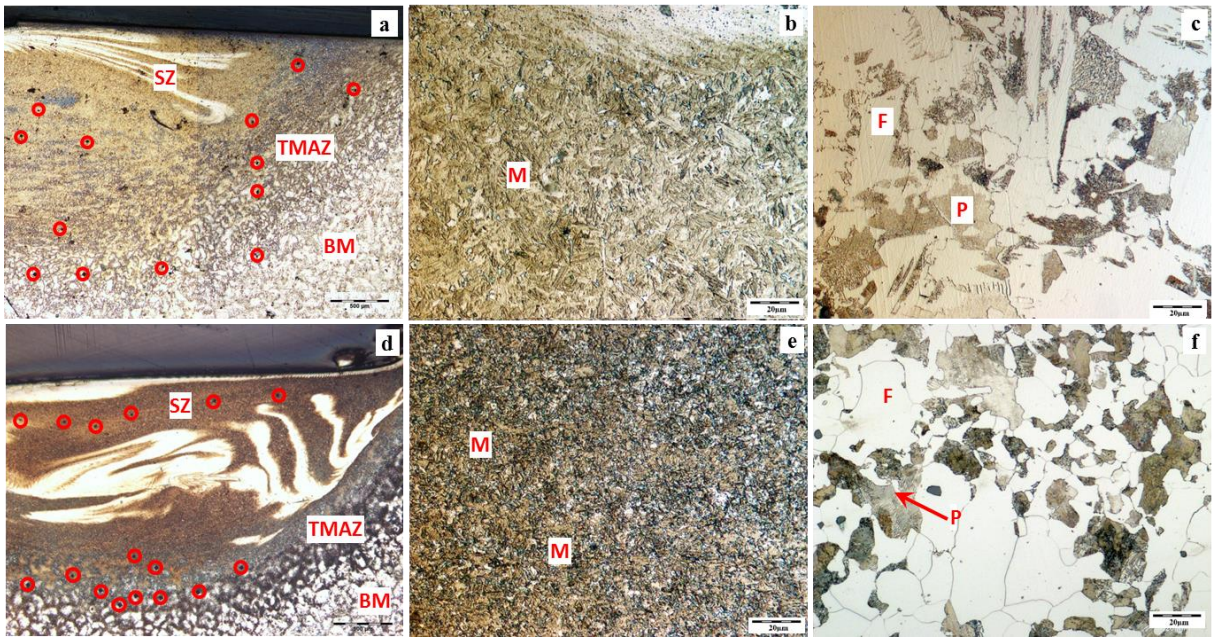

Figure 2. OM images of microstructure of base steel and FSPed samples; P1 Sample: a) General view of the FSPed area, b) the structure of the SZ, c) the structure of the TMAZ region; P3 Sample: d) general view of the FSPed area, e) The structure of the SZ, f) Structure of BM. (Hardness measurement locations are marked with red circles. M: Martensite, F: Ferrite, P: Pearlite)

Figure 3 shows scanning electron microscopy images of the SZ, TMAZ, and BM in a P1 sample. Figure 3(a) provides an overview of the area operated in the FSP; Also, the SZ and the TMAZ are marked by red and yellow dashes, respectively. In Figure 3 (b) the general view of the TMAZ area is shown, as can be seen, part of the ferrite structure remains while other parts have become shear structures due to temperature changes and deformation effects around the SZ. The average grain size in a TMAZ is 5 microns. Figure 3(d) shows the parts with shear structure in the TMAZ with higher magnification. Figure 3(c) shows the shear microstructure of the SZ at different magnifications. The microstructure of TMAZ usually consists of fine, equiaxed grains that are formed as a result of dynamic recrystallization caused by severe plastic deformation. Microscopic images in Figure 3(b) show the formation of various structures of ferrite, Widmanstätten ferrite, and ferrite-cementite in the TMAZ. During the process, with increasing temperature in the TMAZ, the Widmanstätten ferrite structure is formed by directional ferrite plates with an aspect ratio higher than 10: 1 at relatively low cooling rates of the austenite area. As a result of severe plastic deformation in the TMAZ, dynamic recrystallization occurs. Thus, the structure of Widmanstätten ferrite is formed with a relatively low displacement density. In previous research; the formation of shear bands of sub-grains perpendicular to the Widmanstätten ferrite plates has been observed due to severe plastic deformation [22, 23]. Cementite layers in the primary microstructure pearlite are fragmented by the stir effect of the rotating pin. Random scattering of fragmented cementite in the ferrite field in different ratios is seen in Figure 3(d). The formation of ferrite-cementite masses begins just before or after the onset of Widmanstätten ferrite growth [23].

Figure 3(c) shows the structure of the SZ at different magnifications. No cavities, porosity, or cracks are observed in the structure and the structure is completely sheared. According to previous research, martensitic conversion may occur during the friction stir process of low-carbon or medium-carbon steels. On the other hand, depending on the peak temperature during the process and the cooling rate, different percentages of martensitic conversion may occur in different stirring regions with severe deformation. During the process, the SZ becomes austenitic because the peak temperature of this region is higher than A3. The austenite phase is converted to layered martensite due to rapid cooling [23]. The predominant structure of layered martensite in this area is seen in the figure. The occurrence of such layered martensite during the friction stir process of low-carbon and medium-carbon steels has also been observed and reported in some previous studies [19,24,25].

Figure 4 shows scanning electron microscope images from different areas in a sample treated in three passes at different magnifications. The structure of different sections (SZ, TMAZ) in P3 is not significantly different from P1, and the distribution and percentage of phases are almost the same.

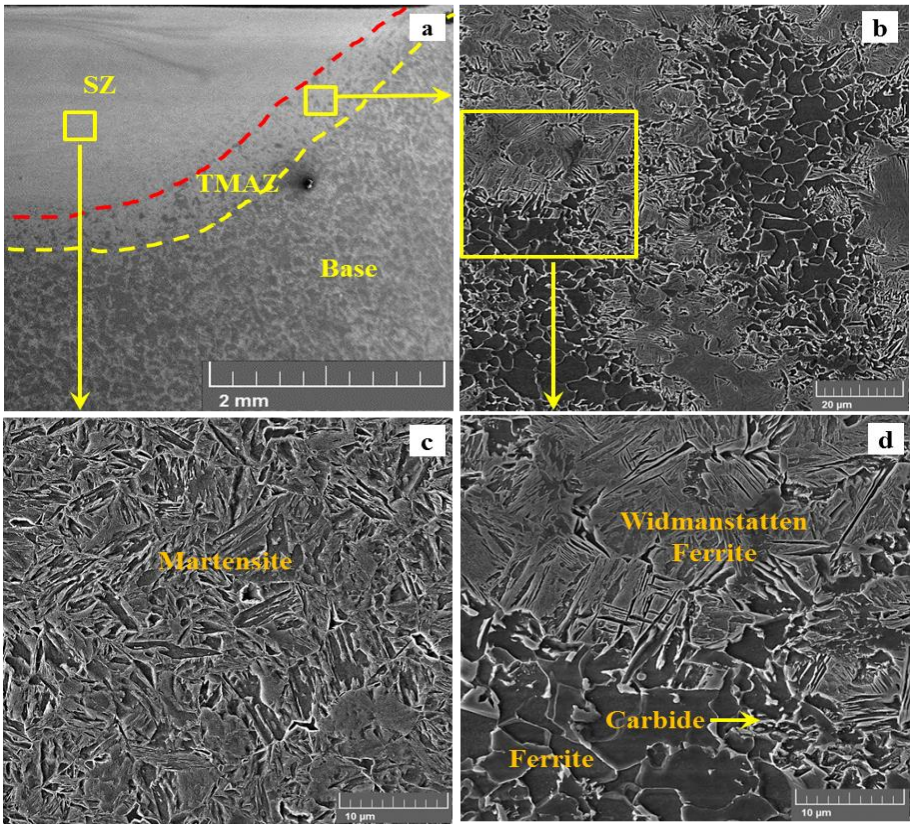

Figure 3. SEM micrograph of P1 sample; a) general view of the FSPed area, (b, d) general view of the TMAZ, (c) the structure of the SZ

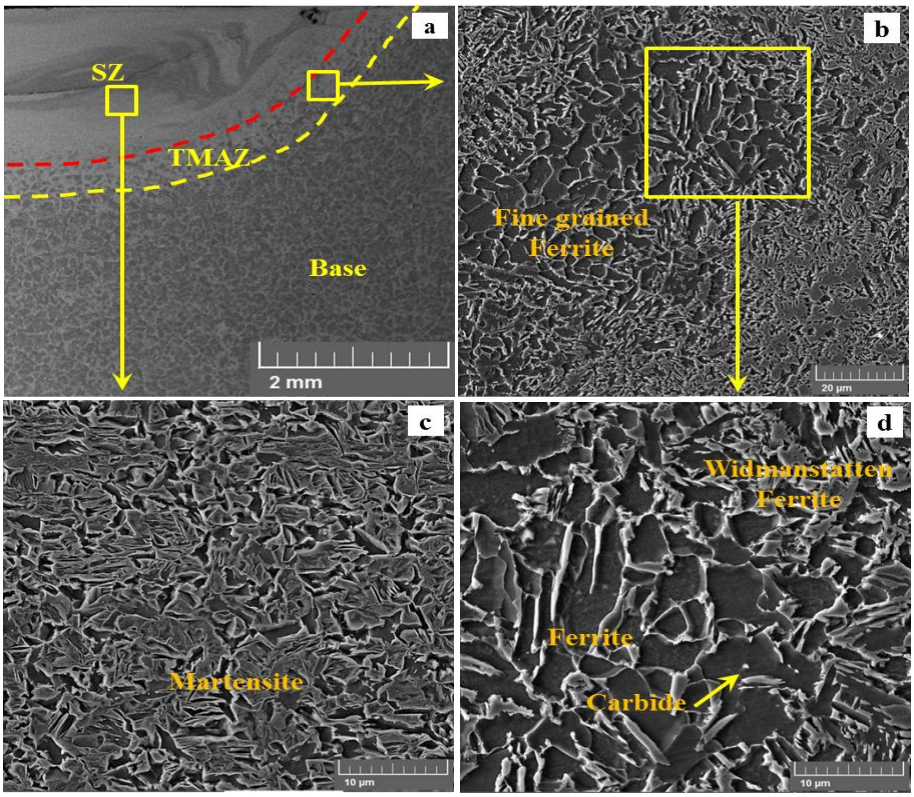

Figure 4. SEM micrograph of P3 sample; (a) general view of the FSPed area, (b, d) general view of the TMAZ, (c) The structure of the SZ

3.2 Microhardness

Figure 5 shows a comparison of the average microhardness of the SZ, TMAZ, and BM for P1 and P3 samples of the friction stir process. While the hardness of the BM is 165 Vickers, by performing the FSP process, the hardness in SZ and TMAZ reaches 785 and 471 Vickers, respectively. The fineness of the grain and phase change to martensite and increase in the density of dislocations is the cause of this increase of up to 4.5 times. As the distance from the center increases, the hardness decreases in proportion to the reduction of deformation, and in TMAZ it is 2.5 times that of the BM [26]. The results of the mechanical properties of the processed samples and the primary metal are shown in Table 1.

Table 1. Results of the mechanical properties of the processed samples and the base metal

Sample	Tensile test			Hardness (HV)		
	$YS_{0.2}$ (MPa)	UTS (MPa)	EL (%)	SZ	TMAZ	BM
P1	310	570	15	784±8.5	471±10.5	207±19
P3	300	530	16	754±13.3	431±33.8	180±5.9
BM	280	460	20	-	-	165

Sample	Wear test (Weight loss (g))				
	600 (m)	1200 (m)	1800 (m)	2400 (m)	3000 (m)
P1	0.0046	0.0081	0.0138	0.0183	0.0275
P3	0.0058	0.0092	0.0157	0.0205	0.0296
BM	0.0138	0.0275	0.0414	0.0546	0.0676

By increasing the number of passes, the possibility of partial tempering of the martensite structure increases, and with recrystallization and grain growth, the hardness decreases. As a result, in the P3 sample, the hardness of the SZ and the TMAZ reaches 754 and 430 HV, respectively. In this sample, in all areas, the hardness is between 30 and 40 Vickers less than the P1 sample. According to the Hall-Petch equation, with decreasing grain size, yield strength and hardness of the material increase. Microstructure modification may lead to a significant increase in microhardness values so that hardness is inversely related to grain size square root. Other researchers have studied the application of FSP on the surface of steels and concluded that the higher surface hardness by FSP is due to two mechanisms, mainly phase transformation and grain size reduction [27, 28]. The higher hardness in the SZ of all operated specimens may be due to the impact of the tool (non-consumable-tungsten carbide). In the present study, the reduction of grain size, phase transformation, and carbon solubility during the phase change from austenite to martensite in the SZ has led to an increase in hardness which is similar to previous studies [27, 28].

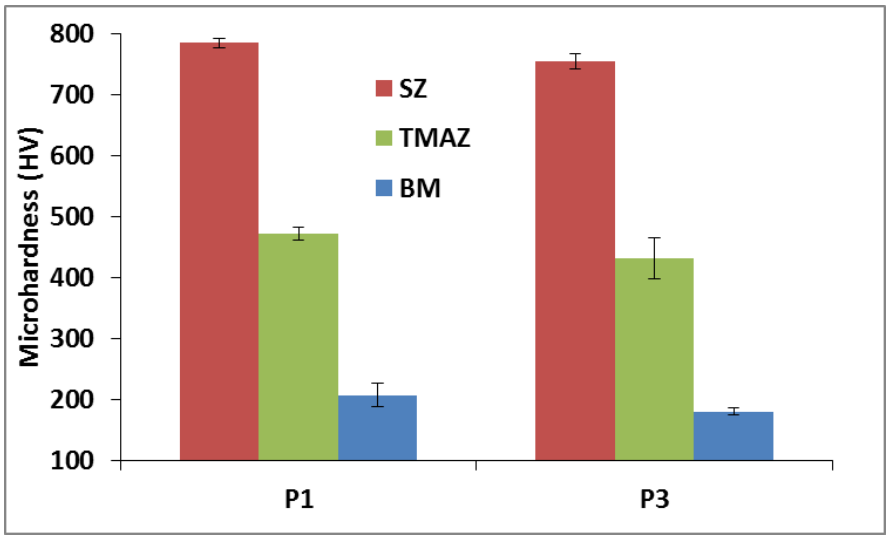

Figure 5. Comparison of average microhardness of SZ, TMAZ, and BM for P1 and P3 samples

3.3 Tensile Test

The Stress vs Strain graphs of the base and FSPed A 216 steel are shown in Fig. 6 and table 1. It is that the yield strength ($YS_{0.2}$) and ultimate tensile strength (UTS) got enhanced after FSPed for P1 and P3 samples and ductility was reduced by a significant extent for all FSPeds samples. The possible rationale for the improvement in mechanical properties of FSPed A216 may be recognized as the microstructural grain size modification. It has been found that the FSP specimens have moderately higher yield strength (YS) and ultimate strengths (UTS) but tremendously lower elongations than the parent metal. The YS and UTS have shown experimental values for the BM as 283 MPa and 462 MPa respectively, and ductility was 20.5%. After FSP, higher YS of 310 MPa and 302 MPa were obtained for P1 and P3 respectively. Moreover, the UTS of 575 MPa and 534 MPa were obtained in the processed zone for P1 and P3 samples respectively. The ultimate tensile strength was improved by 24% and 15.2% for P1 and P3 samples respectively as compared to base steel, however, the elongation decreased to about 25.5 % and 20.2 % for P1 and P3 respectively.

Sample P1 showed the lowest elongation and the highest strength because it had more martensite and shear structures. On the other hand, increasing the number of passes leads to a decrease in YS and UTS compared to the P1 sample and a slight increase in ductility; which corresponds to the partially tempering of the martensite structure due to the input heat of the second and third passes. In literature, similar behavior has been observed in the change of strength and ductility of FSP samples [23,29]. The martensite phase is rapidly formed due to quenching in the stirred region and this tendency increases with the increase of carbon percentage. The increase in hardness and strength of FSPed samples can also be attributed to the modification of the grain structure. When the grain size decreases, the grain boundary region increases. Grain boundaries prevent the movement of dislocations in the processed regions. Therefore, the increase in strength is due to the increment of the grain boundary region. Stiffness-strength and elongation usually have opposite behavior. Decreasing the grain size from 25 μm to 3 μm reduces the effective slip space and increases the number of dislocations along the grain boundaries, i.e. when slip is delayed, the strain rate increases. A higher concentration of dislocations in SZ can lead to a change in strain hardening in the processed samples compared to the parent metal. In addition, the homogeneity of plastic deformation in fine-

grained structures may also be the main reason for the slight reduction in ductility of the processed samples. The smaller the grains, the lower the ability of the grain to deform, and thus the dislocation density increases. Therefore, the saturation of dislocation density in the grains of the SZ can also lead to the reduction of ductility.

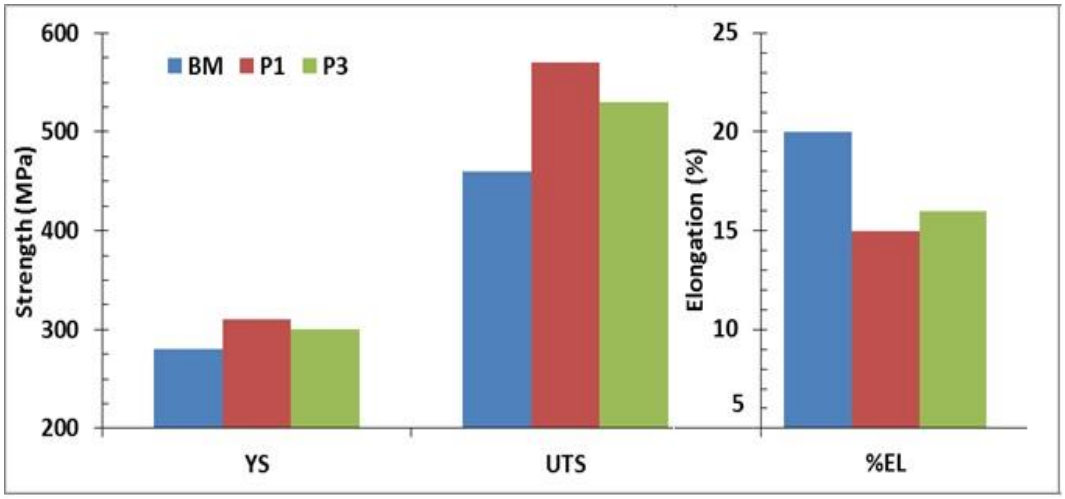

Figure 6. Stress-Strain Curve for BM and FSPed samples

3.4 Wear test

Figure 7 and table, 1show the total weight loss of the samples in terms of distance traveled in the wear test. According to this diagram, it can be seen that the weight loss values of the BM sample and FSPed samples, after 3000 m wear distance, were measured as 67.6 and 27.5 mg, respectively. The weight loss of the BM is about 250% higher than that of the FSPed samples. The reason for the high weight loss of the BM sample is due to its ferrite-pearlite structure. In FSPed samples, the higher the hardness and shear structure, the lower the amount of weight loss in the wear test. The presence of the martensite phase along with the reduction of grain size makes an acceptable improvement in the wear rate of the FSPed sample compared to the BM sample. As previously stated, hardness and strength increased significantly after FSP, especially within the SZ. This increase in hardness increases the resistance to plastic during wear and thus increases the wear resistance of the material [30, 31].

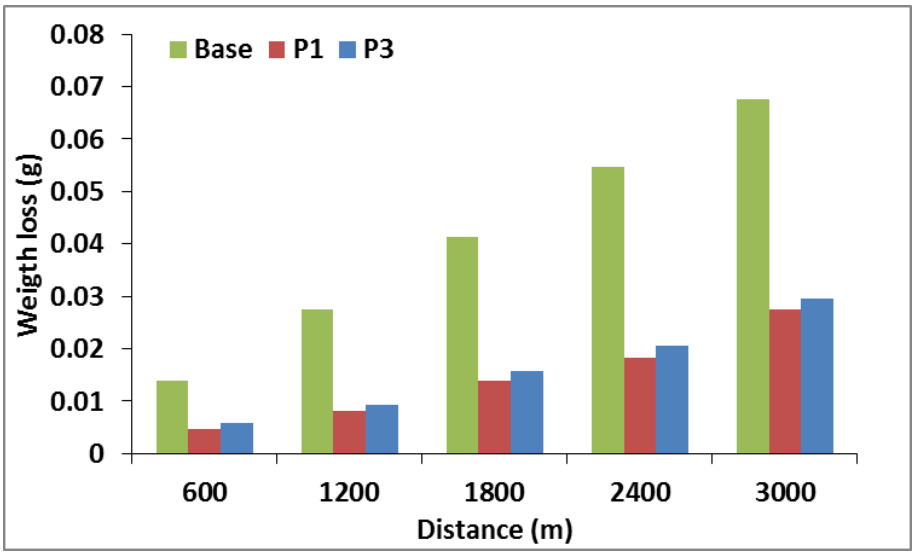

Figure 7. Weight loss changes in terms of slip distance of BM, P1, and P3 samples

At an applied load of 80 kg-force and due to the generated heat affected by friction, adhesive bonds are formed. It is unavoidable to prevent the formation of adhesive bonds when the surfaces are close to each other, and on the other hand, the connection causes the unevenness of the harder material to sink into the softer material [25]. In such a situation, due to the sliding movement on the surface, the material is moved to the front and around, it forms grooves in the direction of movement in the form of scratches on the surface, which creates a mechanism of the scratch type (Figure 8).

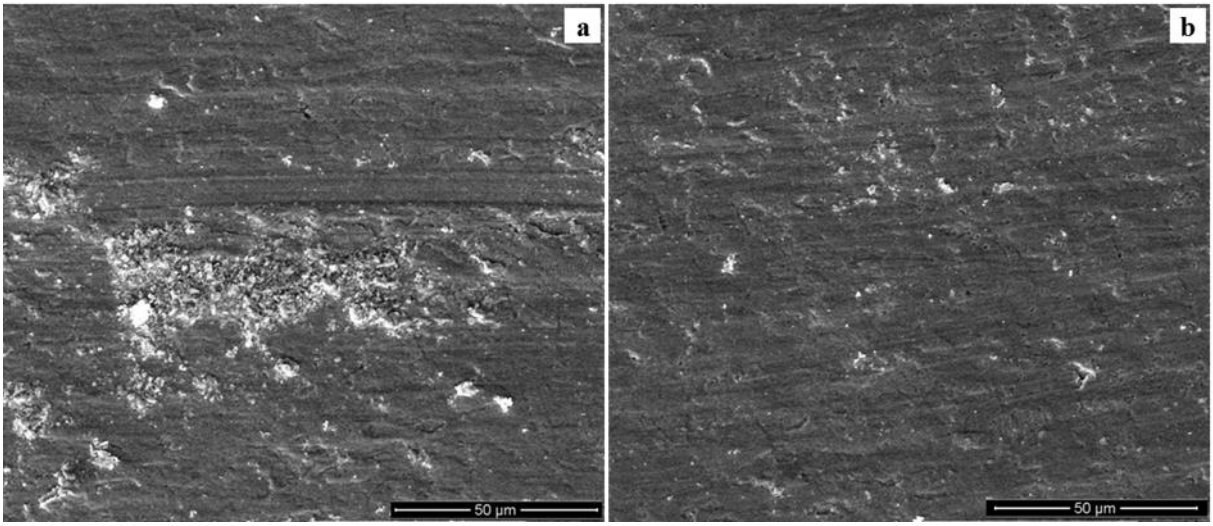

Figure 8. SEM micrograph of the wear surface after 3000 m wear; (A) BM, (b) P1 sample

4. Conclusion

In this research, the friction stir process was performed on cast steel sheet A216 with a tungsten carbide tool, with a rotation speed of 2800 rpm, and advance speed of 80 mm/min, in two modes of one pass and three passes in a water environment with a temperature of 5 °C. By examining the microstructure, microhardness, and abrasion behavior of the SZ, TMAZ, and BM; the following results were obtained: By performing FSP, the average grain size in the P1 sample is reduced from 25 microns in BM to 3 and 5 microns in SZ and TMAZ, respectively. Grain refining by the Hall-

Petch equation and the phase transformation from austenite to martensite phase increases the hardness by 4.5 and 2.5. In the P3 sample, the hardness is between 30 and 40 Vickers less than in the P1 sample. Yield strength improved by 10.5 and 7% and tensile strength increased by 24 and 15.2%, and elongation reduced by 25 and 20% respectively for P1 and P3. Compared to the BM, the weight loss due to wearing in the SZ region improves by 250% and reaches 27.5 and 29.6 mg, respectively for P1 and P3 at 3000 meters. By increasing the number of passes, the hardness, wear resistance, and strength decrease to some extent with the increase in the probability of recovery of shear structures and recrystallization.

5. Acknowledgment

This work was supported by Arak Godazesh Company.

6. References

[1] Sun, Y., Fujii, H. and Morisada, Y. 2020. Double-sided friction stir welding of 40 mm thick low carbon steel plates using a pcBN rotating tool. Journal of Manufacturing Processes. 50: 319-328

[2] Neville, A. and Wang, C. 2009. Erosion–corrosion of engineering steels-Can it be managed by use of chemicals? Wear. 267(11): 2018-2026.

[3] Zhao, W., Zhang, T., Wang, Y., Qiao, J. and Wang, Z. 2018. Corrosion failure mechanism of associated gas transmission pipeline. Materials. 11(10): 1935.

[4] Merah, N., Abdul Azeem, M., Abubaker, H.M., Al-Badour, F., Albinmousa, J. and Sorour., A.A. 2021. Friction Stir processing influence on microstructure, mechanical, and corrosion behavior of steels: A review. Materials. 14(17): 5023.

[5] Mohan, D.G. and Wu, C. 2021. A review on friction stir welding of steels. Chinese Journal of Mechanical Engineering. 34(1): 1-29.

[6] Bhardwaj, N., Ganesh Narayanan, R., Dixit, U.S. and Hashmi, M. S. J. 2019. Recent developments in friction stir welding and resulting industrial practices. Advances in Materials and Processing Technologies. 5(3): 461-496.

[7] Akbari, M., Asadi, P. and Rahimi Asiabaraki, H. 2021. Improving the Hardness and Microstructural Properties of Piston Alloy Using the FSP Method. Journal of Modern Processes in Manufacturing and Production. 10(2): 53-62.

[8] Zykova, A. P., Tarasov, S. Y., Chumaevskiy, A. V. and Kolubaev, E. A. 2020. A review of friction stir processing of structural metallic materials: Process, properties, and methods. Metals. 10(6):772.

[9] Nandan, R. G. G. R., Roy, G. G., Lienert, T. J. and Debroy, T. 2007. Three-dimensional heat and material flow during friction stir welding of mild steel. Acta materialia. 55(3): 883-895.

[10] Wu, L.H., Hu, X.B., Zhang, X. X., Li, Y. Z., Ma, Z. Y. , Ma, X.L. and Xiao, B. L. 2019. Fabrication of high-quality Ti joint with ultrafine grains using submerged friction stirring technology and its microstructural evolution mechanism. Acta Materialia. 166: 371-385

[11] Cui, L., Fujii, H., Tsuji, N., Nakata, K., Nogi, K., Ikeda, R. and Matsushita, M. 2007. Transformation in stir zone of friction stir welded carbon steels with different carbon contents. ISIJ International. 47(2): 299-306.

[12] Choi, D. H., Lee, C. Y., Ahn, B. W., Choi, J. H., Yeon, Y. M., Song, K. Park, H. S., Kim, Y. J. Yoo, C. D. and Jung, S. B. 2009. Frictional wear evaluation of WC–Co alloy tool in friction stir spot welding of low carbon steel plates. International Journal of Refractory Metals and Hard Materials. 27(6):931-936.

[13] Escobar, J. D., Velásquez, E., Santos, T. F. A., Ramirez, A. J. and López, D. 2013. Improvement of cavitation erosion resistance of a duplex stainless steel through friction stir processing (FSP). Wear. 297(1-2): 998-1005.

[14] Grewal, H. S., Arora, H. S., Singh, H. and Agrawal, A. 2013. Surface modification of hydroturbine steel using friction stir processing. Applied Surface Science. 268: 547-555.

[15] Aldajah, S. H., Ajayi, O. O., Fenske, G. R. and David, S. 2009. Effect of friction stir processing on the tribological performance of high carbon steel. Wear. 267(1-4): 350-355.

[16] Chen, Y. C. and Nakata, K. 2009. Evaluation of microstructure and mechanical properties in friction stir processed SKD61 tool steel. Materials characterization. 60(12):1471-1475.

[17] Chabok, A. and Dehghani, K. 2013. Effect of processing parameters on the mechanical properties of interstitial free steel subjected to friction stir processing. Journal of Materials Engineering and Performance. 22(5):1324-1330.

[18] Mehranfar, M. and Dehghani, K. 2011. Producing nanostructured super-austenitic steels by friction stir processing. Materials Science and Engineering: A. 528(9): 3404-3408.

[19] Dodds, S., Jones, A. H. and Cater, S. 2013. Tribological enhancement of AISI 420 martensitic stainless steel through friction-stir processing. Wear. 302(1-2): 863-877.

[20] Singh, S., Kaur, M. and Saravanan, I. 2020. Enhanced microstructure and mechanical properties of boiler steel via Friction Stir Processing. Materials Today: Proceedings. 22:482-486.

[21] Singh, S., Kaur, M. and Kumar, M. 2020. A Novel Technique for Surface Modification of SA 210 Gr A1 Steel. Materials Today: Proceedings. 21: 1930-1936.

[22] Sekban, D. M., Aktarer, S. M., Yanar, H., Alsaran, A. and Purcek, G. 2017. Improvement the wear behavior of low carbon steels by friction stir processing. In IOP Conference Series: Materials Science and Engineering.174 (1):012058.

[23] Xue, P., Xiao, B. L., Wang, W. G., Zhang, Q., Wang, D., Wang, Q. Z. and Ma, Z. Y. 2013. Achieving ultrafine dual-phase structure with superior mechanical property in friction stir processed plain low carbon steel. Materials Science and Engineering: A, 575: 30-34.

[24] Sekban, D. M., Aktarer, S. M. and Purcek, G. 2019. Friction stir welding of low-carbon shipbuilding steel plates: microstructure, mechanical properties, and corrosion behavior. Metallurgical and Materials Transactions A. 50(9): 4127-4140.

[25] Wang, H., Wang, K., Wang, W., Lu, Y., Peng, P., Han, P. and Wang, L. 2020. Microstructure and mechanical properties of low-carbon Q235 steel welded using friction stir welding. Acta Metallurgica Sinica (English Letters). 33(11):1556-1570.

[26] Wang, Z. W., Ma, G. N., Yu, B. H., Xue, P., Xie, G. M., Zhang, H. and Ma, Z. Y. 2020. Improving mechanical properties of friction-stir-spot-welded advanced ultra-high-strength steel with additional water cooling. Science and Technology of Welding and Joining. 25(4): 336-344.

[27] Costa, M. I., Verdera, D., Vieira, M. T. and Rodrigues, D. M. 2014. Surface enhancement of cold work tool steels by friction stir processing with a pinless tool. Applied surface science. 296: 214-220.

[28] Lorenzo-Martin, C. and Ajayi, O. O. 2015. Rapid surface hardening and enhanced tribological performance of 4140 steel by friction stir processing. Wear. 332: 962-970.

[29] Singh, S., Kaur, M., Kumar, M., Singh, H. and Singh, S. 2019. Study of microstructure evolution, mechanical properties and hot corrosion behavior of friction stir processed boiler steel. Materials Research Express. 6(9): 096547.

[30] Xue, P., Li, W. D., Wang, D., Wang, W. G., Xiao, B. L. and Ma, Z. Y. 2016. Enhanced mechanical properties of medium carbon steel casting via friction stir processing and subsequent annealing. Materials Science and Engineering: A. 670: 153-158.

[31] Hajian, M., Abdollah-Zadeh, A., Rezaei-Nejad, S. S., Assadi, H., Hadavi, S. M. M., Chung, K. and Shokouhimehr, M. 2015. Microstructure and mechanical properties of friction stir processed AISI 316L stainless steel. Materials & Design. 67: 82-94.